Ocean Color Optical Property Data Derived from OCTS and POLDER: A Comparison Study

Menghua Wang[1], Alice Isaacman[2], Bryan A. Franz[2], and
Charles R. McClain

Code 970.2, NASA Goddard Space Flight Center
Greenbelt, Maryland 20771, USA
[1]University of Maryland Baltimore County
[2]SAIC General Sciences Corporation

Submitted to *Applied Optics*

(3/5/01)

Acknowledgments

ABSTRACT

We describe our efforts in studying and comparing the ocean color data derived from the Japanese Ocean Color and Temperature Scanner (OCTS) and the French Polarization and Directionality of the Earth's Reflectances (POLDER). OCTS and POLDER were both on board Japan's Sun-synchronous Advanced Earth Observing Satellite (ADEOS-1) from August 1996 to June 1997, collecting about 10 months of global ocean color data. This provides a unique opportunity for developing methods and strategies for the merging of ocean color data from multiple ocean color sensors. In this paper, we describe our approach in developing consistent data processing algorithms for both OCTS and POLDER and using a common in situ data set to vicariously calibrate the two sensors. Therefore, the OCTS and POLDER-measured radiances are effectively bridged through common in situ measurements. With this approach in processing data from two different sensors, the only differences in the derived products from OCTS and POLDER are the differences inherited from the instrument characteristics. Results show that there are no obvious bias differences between the OCTS and POLDER-derived ocean color products, whereas the differences due to noise, which stem from variations in sensor characteristics, are difficult to correct. It is possible, however, to reduce noise differences with some data averaging schemes. The ocean color data from OCTS and POLDER can therefore be compared and merged in the sense that there is no significant bias between two.

1. Introduction

The Japanese Ocean Color and Temperature Scanner (OCTS)[1] and French Polarization and Directionality of the Earth's Reflectances (POLDER)[2] were both flown on the Japanese Sun-synchronous Advanced Earth Observing Satellite (ADEOS-1) from August 1996 to June 1997, collecting about 10 months of global ocean color data. ADEOS-1 was on a polar orbit at an altitude of 800 km with local crossing time (descending node) at around 10:40 AM. This was the first time in history that two ocean color sensors were on board the same platform and viewed the global ocean with the same temporal and similar global spatial coverages. Therefore, it provides an ideal case for studying and comparing ocean color data derived from two different sensors, hence allowing development of a strategy for ocean color data merger from multiple ocean color sensors. The primary goal of the NASA Sensor Intercomparison and Merger for Biological and Interdisciplinary Oceanic Studies (SIMBIOS) project is to develop methods for meaningful comparison and merging of data products from multiple ocean color missions.[3] In a recent study, Wang and Franz[4] show that, using a vicarious inter-calibration approach between the modular optoelectronic scanner (MOS)[5] and the Sea-Viewing Wide Field-of-View Sensor (SeaWiFS)[6,7] (SeaWiFS ocean color data used as "truth"), the ocean optical property data derived from two sensors can be meaningfully compared. The bias differences are significantly reduced between the two products. In that study,[4] measurements from the two sensors had a temporal difference of about 90 minutes. In this paper, we compare the ocean color data derived from OCTS and POLDER measurements using consistent data processing algorithms for both sensors and vicarious calibrations based on a common in situ data set from the Marine Optical Bouy (MOBY).[8] Therefore, differences in the derived ocean color products from OCTS and POLDER are primarily associated with differences in instrument characteristics. We first give a brief overview of the sensor characteristics of the OCTS and the POLDER and their differences. Detailed al-

1

gorithm descriptions for processing OCTS and POLDER data are then presented. Next, we outline the vicarious calibration scheme in which the OCTS and POLDER measured radiances are calibrated using a common in situ MOBY data set. Finally, we provide results comparing OCTS and POLDER ocean color data with global in situ measurements, and compare a series of OCTS measurements with those of POLDER over the Sargasso Sea and the Bermuda area.

2. Instrument Characterizations

OCTS, which was built and operated by the National Space Development Agency (NASDA) of Japan, is an optical radiometer[1] with a scanning swath of 1400 km and a spatial resolution at nadir of 0.7 km. OCTS has 8 spectral bands (out of 12) for ocean color measurement centered at wavelengths 412, 443, 490, 520, 565, 670, 765, and 865 nm. The bandwidths of the first 6 bands are 20 nm and those of the last two near-infrared (NIR) bands are 40 nm. The NIR bands can be used for the atmospheric corrections.[9-11] In addition, OCTS has a capability of operationally tilting the sensor ±20° away from nadir to minimize sun glint contamination. In comparison, POLDER, which was built and operated by the Centre National d'Etudes Spatiales (CNES) of France, is a multi-angle imaging radiometer/polarimeter with a 242×274 CCD pushbroom matrix array.[2] POLDER has a wide field of view (2400 km), a spatial resolution at nadir of ~6-7 km, and 6 spectral bands centered at 443, 490, 565, 670, 765, and 865 nm for ocean color measurement. The bandwidths of the first four visible bands are 20 nm and those of the two NIR bands are 40 nm. Both 670 and 865 nm bands are designed to measure the polarized radiance in addition to another 443 nm polarized band. For a given earth ground scene (target), POLDER can provide up to 14 near-contemporaneous measurements at various viewing directions, therefore it is useful for deriving atmosphere and/or ground bi-directional reflectance distribution functions (BRDF). Obviously, these two sensors have many different design characteristics, even though their main goal of retrieving the

global ocean color products is the same. For that purpose, they have 6 common spectral bands at 443, 490, 565, 670, 765, and 865 nm.

3. Algorithm Descriptions

The data processing algorithms used for OCTS and POLDER are described in the following two sections. The processing algorithms are implemented in the Multi-Sensor Level-1 to Level-2 (MSL12) software which is freely distributed as part of SeaWiFS Data Analysis System (SeaDAS) software package.[12]

A. Data Processed to Level-1B

The OCTS and POLDER Level-1B data are usually obtained from Japan's NASDA and the French CNES data centers. However, during the ADEOS-I mission lifetime, approximately 450 GB of real-time OCTS data were collected by the SeaWiFS project through the National Oceanic and Atmospheric Administration (NOAA) ground stations at Wallops, Virginia and Fairbanks, Alaska. Since standard OCTS Level-0 to Level-1B software was not publicly available, the SIMBIOS project engaged in developing and enhancing the Level-0 to Level-1B processing software, with specific attention given to improving geolocation and image registration. Herein, we briefly describe the OCTS Level-0 to Level-1B processing software developed by the SIMBIOS project.

In general, the processing of Level-0 data to Level-1B includes conversion of raw sensor counts to physical units and the assignment of geolocation information to each observation (pixel, detector, and band). Several factors in the design of the OCTS instrument complicate this process. Each OCTS band is divided into 10 individual detectors, where each detector is associated with a separate scan line. Each detector has a slightly different and apparently non-linear responsivity, which gives rise to horizontal striping in the OCTS imagery.[13] The basis for the SIMBIOS calibration is the NASDA Version 3 preflight calibration and relative detector calibration.[14] The relative detector calibration substantially reduces the striping effects, but low-level artifacts are still visible and they

can become significant following removal of the large, comparatively smooth atmospheric signal.

The design of the OCTS scan mirror and focal plane results in severe misalignment of the line-of-sight for different spectral bands viewing at essentially the same time.[13] To perform atmospheric correction or derive chlorophyll concentration at a given location requires that the bands be co-registered to that location. The SIMBIOS project developed a registration technique in which an idealized focal-plane geometry is defined, and all bands are resampled using a nearest neighbor approach to match the idealized ground track. This method is similar in concept to the approach of using OCTS band 1 as a nearest neighbor matching target,[13] but it also eliminates scan to scan overlap. Furthermore, while the registration process can correct for differences in geolocation between bands, the resampled observations come from different lines-of-sight with unique sensor-to-ground and Sun-to-ground geometries. To ensure accurate atmospheric correction, the true solar and sensor view angles for each band are saved in the Level-1B file for use in the Level-1B to Level-2 processing. Note that this is not possible with NASDA standard Level-1B products because only nominal angles are saved.

Before the registration process can begin, however, the observations from each band must be accurately navigated. The geolocation algorithm used for SIMBIOS OCTS processing is a modified version of the method used for SeaWiFS navigation.[15] This technique has the potential to yield an exact solution to the geolocation of each scan line when the spacecraft position and sensor geometry are accurately known. To improve geolocation accuracy, the SIMBIOS project derived time-dependent attitude and tilt adjustments using an automated navigation assessment technique based on island targets.[16] Results show that, using the SIMBIOS Level-1B data processing, the OCTS navigation is accurate to approximately one kilometer.

The OCTS Level-1B data processed with the SIMBIOS code usually agree well with the NASDA standard Level-1B product. For OCTS bands 1-8, the radiance frequency

distributions from the two processes are nearly identical. However, the radiance differences based on a *pixel by pixel* comparison can disagree due to small differences in navigation and band coregistration, i.e., in such comparisons, the corresponding pixels from the NASDA standard Level-1B and the SIMBIOS Level-0 to Level-1B routine are usually not the same. In a typical example, these differences were found to be 0.54%, 0.53%, 0.54%, 0.85%, 1.00%, 1.62%, 2.20%, and 2.67% for bands 1-8, respectively.

B.   Data Processed from Level-1B to Level-2

For ocean color remote sensing, Level-1B to Level-2 data processing mainly involves the atmospheric correction,[9-11,17,18] in which the radiance contributions from the atmosphere and ocean surface as well as their interactions are removed from the sensor-measured signals at the top of the atmosphere (TOA). The radiance contributions from the ocean, i.e., the water-leaving radiances just above the sea surface, can then be retrieved. A simple empirical algorithm[19-21] can then be used to derive the ocean chlorophyll concentration from the normalized water-leaving radiances. In the following, a consistent atmospheric correction algorithm applied to OCTS and POLDER as well as a bio-optical algorithm tuned to OCTS and POLDER spectral bands are briefly described. The data processing procedures, in particular for POLDER, are outlined.

1.   Atmospheric Corrections

Based on a study by Wang,[22] the SIMBIOS project has developed the MSL12 software for processing data from multiple ocean color sensors. MSL12 is an implementation of the standard SeaWiFS atmospheric correction algorithm,[9,17] with some generalizations to allow for application to OCTS, POLDER, and other ocean color sensors (e.g., MOS).[4,22] Therefore, a consistent atmospheric correction algorithm can be used to process data from OCTS and POLDER.

Similar to SeaWiFS, both OCTS and POLDER have two NIR bands at 765 and 865 nm for the atmospheric correction. However, the 765 nm spectral band completely en-

compasses the oxygen A-band absorption. Figure 1 compares the OCTS and POLDER 765 nm band spectral response functions (SRF) with that of SeaWiFS. Clearly, both OCTS and POLDER 765 nm band SRFs are almost identical to that of SeaWiFS. Therefore, the same SeaWiFS oxygen A-band absorption correction algorithm[23] can be used for both OCTS and POLDER. A small difference in the SRFs (mainly between POLDER and SeaWiFS) is within the uncertainty of the correction algorithm.[23,24]

There are some major improvements in MSL12 for the OCTS and POLDER data processing which are concurrent with changes in processing algorithms for the SeaWiFS 3rd data reprocessing in May 2000.[25] Some specific atmospheric correction algorithm improvements include:

1. An iterative correction algorithm, which accounts for the ocean radiance contributions at two NIR wavelengths (765 and 865 nm), was developed and implemented in the data processing.[26]

2. Improved Rayleigh radiance lookup table, in which the Rayleigh (air molecules) scattering radiance is a function of the sea surface wind speed (in addition to solar and sensor viewing geometry and wavelength dependence),[27] was generated and implemented in the MSL12 data processing system[28] for OCTS and POLDER.

3. A sun glint contamination correction algorithm, which effectively removes the sun glint residual contamination radiance around the sub-solar point, was developed and implemented in MSL12.[29]

4. Correction of the ocean whitecap radiance contributions[17] was updated[25] using some current in situ measurements.[30-32]

5. The current 12 aerosol models used in generating aerosol lookup tables for the atmospheric correction are: Oceanic with relative humidity (RH) of 99%, Maritime with RH of 50%, 70%, 90%, and 99%, Coastal with RH of 50%, 70%, 90%, and 99%, and Tropospheric with RH of 50%, 90%, and 99%.[25] The Oceanic, Maritime, and Tro-

pospheric models are from Shettle and Fenn,[33] whereas the Coastal model was derived using data from the Shettle and Fenn models.[9]

6. A correction algorithm for the sensor spectral bandpass effects on the derived normalized water-leaving radiances for SeaWiFS[34] was developed. Similar algorithms for both OCTS and POLDER were also implemented in MSL12. Similar to Wang et. al. (Figure 3 (b)),[34] Figures 2(a) and 2(b) provide the spectral bandpass correction factor $r(\lambda)$ as a function of the sensor-derived (uncorrected) ratio values between the normalized water-leaving radiances at wavelengths 490 and 565 nm. Note that $r(\lambda) > 1$ indicates under-estimation of the derived normalized water-leaving radiance $[L_w(\lambda)]_N$, whereas $r(\lambda) < 1$ indicates over-estimation. Fig. 2(a) shows the correction factors for the OCTS's spectral bands, while Fig. 2(b) shows those for POLDER. Fig. 2(a) shows that, without corrections, the OCTS-derived $[L_w(\lambda)]_N$ at 565 nm is under-estimated (~8%), while the values at 520 nm are over-estimated (up to ~17%) for clear ocean waters. Other OCTS bands (412, 443, and 490 nm) have almost no spectral bandpass effects. On the other hand, without corrections, the POLDER 490 nm band has ~5% under-estimation for the derived value in clear ocean waters, while for the 565 nm band there is under-estimation from about 3.5%-1.5% of the derived values for ocean waters ranging from productive to non-productive (clear) cases. Clearly, corrections of the sensor spectral bandpass effects are necessary in order to have a meaningful Level-2 product comparison derived from two different sensors, e.g., OCTS and POLDER.

2. *Bio-Optical Algorithms*

In this study, we use the bio-optical algorithm of ocean chlorophyll 2 (OC2)[21] for deriving the ocean chlorophyll concentration from the sensor-retrieved normalized water-leaving radiance $[L_w(\lambda)]_N$. Therefore, a consistent bio-optical algorithm is used in deriving chlorophyll concentration for both OCTS and POLDER. The OC2 algorithm was modified by O'Reilly and Maritorena (per. comm.) to account for the effects of the spec-

tral band differences between the OCTS and POLDER 565 nm band and the SeaWiFS 555 nm band, i.e.,

$$Chl = 10^{\left(0.3164 - 2.132R + 0.6303R^2 + 0.004R^3\right)} - 0.0708, \qquad (1)$$

where

$$R = \left[\rho_w(490)\right]_N / \left[\rho_w(565)\right]_N \qquad (2)$$

is the ratio between the normalized water-leaving reflectances at 490 and 565 nm. The normalized water-leaving reflectance, $\left[\rho_w(\lambda)\right]_N$, is defined as

$$\left[\rho_w(\lambda)\right]_N = \pi\left[L_w(\lambda)\right]_N / F_0(\lambda), \qquad (3)$$

where $\left[L_w(\lambda)\right]_N$ is the sensor-derived normalized water-leaving radiance and $F_0(\lambda)$ is the extraterrestrial solar irradiance.

3. A Specific Data Processing Procedure for POLDER

As we discussed in previous sections, for a given location (scene), POLDER can acquire as many as 14 near-contemporaneous measurements. Therefore, up to 14 values of the Level 2 product for the same ocean scene can be derived. However, it was noted that, for a given scene, the POLDER derived products, e.g., normalized water-leaving radiances, often have high variations (up to an order of magnitude) between various POLDER viewing directions. These variations are possibly related to the POLDER sub-pixel cloud contamination and/or band non-linear responses.[35] It was also found that, for a given scene, there was no obvious correlation between the POLDER-derived $\left[L_w(\lambda)\right]_N$ and its viewing direction (angle). Therefore, we used an averaging scheme to eliminate points with high variation and to reduce data noise in the derived product. First, for a given pixel, the derived normalized water-leaving radiances from all possible POLDER viewing directions were averaged. Data points which were within 50% variation of the first averaged value (i.e., 0.5-1.5 of average value) were then used to derive the final mean value and considered as the POLDER-derived normalized water-leaving radiances

for the pixel. This averaging scheme was used in deriving the POLDER vicarious gain coefficients, as well as the POLDER Level 2 products.

4. Vicarious Calibrations with MOBY in situ Measurements

It is well known that, for ocean color remote sensing, an on-orbit vicarious calibration of sensor and algorithms is necessary.[36] Vicarious calibration techniques have been successfully applied to SeaWiFS[37,38] and also used to inter-calibrate MOS and SeaWiFS data.[4] In this study, a vicarious calibration for OCTS and POLDER using the in situ measurements from the MOBY[8] was carried out. The sensor vicarious gain coefficients, $G^{(VC)}(\lambda)$, are defined through

$$L_t^{(VC)}(\lambda) = G^{(VC)}(\lambda) L_t^{(meas)}(\lambda), \qquad (4)$$

where $L_t^{(meas)}(\lambda)$ is sensor-measured Level-1B radiance from OCTS and POLDER and $L_t^{(VC)}(\lambda)$ is vicariously calibrated radiance which is used in the Level-1B to Level-2 algorithms as the correct value of $L_t(\lambda)$. The vicarious calibration procedure was proceeded as follows. First, for the 865-nm band, it was assumed that gain coefficients were not changed. They were equivalent to the values suggested by NASDA and CNES. The in-flight gains for OCTS and POLDER 865-nm band were derived by NASDA and CNES as 0.89 and 1.05, respectively.[14,39] Next, the gain coefficient of the 765 nm band was derived by forcing the atmospheric correction algorithm to select a maritime aerosol type over the MOBY site. The procedure was similar to the methods used in adjusting the SeaWiFS 765 nm band.[37] Finally, with the derived 765 nm gain coefficient, the MOBY in situ measurements were used to calibrate the visible bands,[38] i.e., the OCTS and POLDER visible bands were calibrated such that, with the atmospheric corrections, the derived normalized water-leaving radiances were equivalent to the MOBY in situ measurements.

The location of the MOBY site is usually in stable clear-ocean waters and the aerosols are predominantly marine. The MOBY program has been providing consistently high quality clear-ocean optical data since 1997. Unfortunately, there were some problems with the early deployment of MOBY in 1996, limiting the number of usable calibration samples to five measurements spanning the period of November 1996 to February 1997. Specifically, five in situ measurements taken on November 26 of 1996, January 13, January 17, February 16, and February 23 of 1997 were used. Table 1 provides the derived gain coefficients for the OCTS and POLDER spectral bands.

5. Results

Using the derived vicarious gain coefficients, OCTS and POLDER data were processed to Level-2 products from either OCTS Level-0 (data acquired from Wallops, Virginia) and/or OCTS Level-1B data and POLDER Level-1B data using MSL12. As discussed in the previous sections, the processing algorithms for both OCTS and POLDER are essentially the same as for SeaWiFS although some specific modifications are necessary depending on sensor characteristics. In the following four sections, we provide OCTS and POLDER matchup analyses comparing satellite retrievals with in situ measurements, ocean color data comparisons between the two sensors, as well as some data analyses and discussions.

A. Global in situ $\left[L_w(\lambda)\right]_N$ Matchup Analyses

An extensive set of in situ data taken during the time of the OCTS and POLDER missions was archived in the SeaWiFS Bio-optical Archive and Storage System (SeaBASS) data base. These data were used for OCTS and POLDER matchup analyses. In these comparison analyses, the satellite and in situ data were screened and obtained through the following procedure: (i) the differences of time and solar zenith angle between satellite and in situ measurements were less than 4 hours and 15°, respectively; (ii) the solar zenith angle and sensor viewing angle for OCTS and POLDER were ≤ 60°;

(iii) the in situ measurement was between 9 AM to 3 PM local time; (iv) in the matchup analyses, the OCTS $[L_w(\lambda)]_N$ was derived by averaging data in a 5 km circle centered at the location of the in situ measurement, and only data for which a coefficient of determination (the ratio of standard deviation to average) was less than 0.5 were considered; and (v) as discussed previously, POLDER results were derived by first averaging over all possible viewing directions (up to 14 values) and data were then re-averaged after eliminating data points whose differences compared with the first averaged value were > ±50%.

Figures 3 and 4 provide matchup results for the OCTS and POLDER compared with the in situ measurements. Figs. 3(a) and 3(b) show matchup results for the normalized water-leaving radiance $[L_w(\lambda)]_N$ derived from OCTS NASDA standard Level-1B data and Wallops Level-0 data (using SIMBIOS Level-0 to Level-1B processing), respectively. Fig. 4(a) shows the matchup results derived from POLDER CNES Level-1B data compared to the in situ measurements. Figs. 3(c) and 3(d) compare the OCTS derived two-band ratio value $[L_w(\lambda)]_N/[L_w(565)]_N$ from NASDA Level-1B and Wallops Level-0 data, respectively, with results from in situ measurements, while Fig. 4(c) shows the same results from POLDER matchup comparisons. The matchup analyses for the two-band ratio value in the derived $[L_w(\lambda)]_N$ are useful since they are inputs for the ocean color bio-optical algorithms.[19-21]

Results in Figs. 3 and 4 show that, after vicarious calibration using the MOBY data, the derived $[L_w(\lambda)]_N$ and $[L_w(\lambda)]_N/[L_w(565)]_N$ from the OCTS and POLDER measurements compared reasonably well with the in situ data. Note that each plot gives the linear fit showing coefficients of slope, intercept (Int), and the correlation coefficient (R). (A perfect match would have slope of 1, intercept of 0, and the correlation coefficient of 1). It appears, however, that the OCTS-derived $[L_w(\lambda)]_N$ values were slightly over-estimated (slope > 1.0), while the POLDER results were slightly under-estimated (slope < 1.0). The derived two-band ratio values $[L_w(\lambda)]_N/[L_w(565)]_N$ compared better to the in situ

measurements than those of $\left[L_w(\lambda)\right]_N$, indicating that the derived ocean chlorophyll concentrations are reasonably accurate. Results also indicate that the POLDER-derived products are more noisy than the OCTS data since the correlation coefficients derived from the POLDER matches are lower than those from the OCTS comparison.

B. OCTS and POLDER $\left[L_w(\lambda)\right]_N$ Comparisons

A series of measurements from OCTS and POLDER over the Sargasso Sea and the Bermuda area were collected for comparison. The satellite observations were obtained from a co-located 3°×3° box over the Sargasso Sea (latitude of 23.5°N to 26.5°N and longitude of 70°W to 73°W) and the Bermuda area (latitude of 30°N to 33°N and longitude of 62.7°W to 65.7°W). Over the Sargasso Sea and the Bermuda area, OCTS data were all collected through the ground station at Wallops, Virginia. Therefore, OCTS data were processed from Level-0 to Level-1B using the SIMBIOS code, and then to Level-2 using MSL12. Figure 5 provides color images for the OCTS and POLDER derived $\left[L_w(\lambda)\right]_N$ comparisons for wavelengths of 443, 490, and 565 nm over the Sargasso Sea and the Bermuda area. Fig. 5(a) is for the results over the Sargasso Sea, while Fig. 5(b) is for comparisons over the Bermuda area. The color scales for $\left[L_w(\lambda)\right]_N$ images are indicated at the bottom of Fig. 5(b). $\left[L_w(\lambda)\right]_N$ for 443 and 490 nm is scaled from 0 to 3 (mW cm^{-2} μm^{-1} sr^{-1}), while $\left[L_w(\lambda)\right]_N$ for 565 nm is scaled from 0 to 0.8 (mW cm^{-2} μm^{-1} sr^{-1}). In Fig. 5, columns 1-3 are the OCTS-derived $\left[L_w(\lambda)\right]_N$ images for 443, 490, and 565 nm, and columns 4-6 are the POLDER-derived results for 443, 490, and 565 nm. In addition, at the left side of the images, there are indicated dates when OCTS and POLDER measurements were acquired. Over the Sargasso Sea, OCTS and POLDER data were acquired on November 20 and December 19 of 1996, and January 26, February 17, March 11, April 14, and May 20 of 1997 (there were data from each month for seven months), while data were acquired on December 12 of 1996, and March 19, May 3, May 7, and June 10

of 1997 over the Bermuda area. In Fig. 5, each image represents a 3°×3° box over the Sargasso Sea or the Bermuda area.

Results in Fig. 5 show a reasonable agreement between OCTS and POLDER derived $[L_w(\lambda)]_N$ values. Over the Sargasso Sea, both spatial and temporal variations of ocean color were well captured by both OCTS and POLDER. For example, $[L_w(\lambda)]_N$ values at 443 nm changed from November (note the spatial variations in the November image from both OCTS and POLDER) to a lower value in December and January, then elevated in February, and finally reached their highest values in the spring. The spatial $[L_w(\lambda)]_N$ distributions from OCTS and POLDER are comparable. However, there are some obvious differences, e.g., POLDER has a larger pixel size (low spatial resolution) and it appears that the POLDER results show more noisy than results from OCTS. Some sparkling points in the POLDER $[L_w(\lambda)]_N$ images are mostly cloud-edge effects, probably due to sub-pixel cloud contamination because of POLDER low spatial resolution measurement.

Figure 6 compares the histogram (%) of the retrieved $[L_w(\lambda)]_N$ between OCTS and POLDER over the Sargasso Sea and the Bermuda area. Figs. 6(a)-6(g) are comparison results for the Sargasso Sea for data acquired from November 20, 1996 to May 20, 1997, while Figs. 6(h)-6(l) are for the Bermuda area for measurements acquired from December 12, 1996 to June 10, 1997. The OCTS and POLDER $[L_w(\lambda)]_N$ at 490 and 565 nm usually compare quite well, with small variations between the two measurements, while the POLDER $[L_w(\lambda)]_N$ at 443 nm shows significant variations compared with the OCTS results (sometimes high and sometimes low). The shape of the histogram distributions from OCTS and POLDER, however, are generally similar. Table 2 gives quantitative comparisons of the retrieved $[L_w(\lambda)]_N$ between OCTS and POLDER for the mode (peak) values in the histograms, as presented in Fig. 6. Table 2(a) and 2(b) are results for the Sargasso Sea and the Bermuda area, respectively. Although there are some variations in the derived $[L_w(\lambda)]_N$ values between OCTS and POLDER, the average ratio values of

OCTS/POLDER for $[L_w(\lambda)]_N$ 443, 490, and 565 nm for all cases in Table 2 are: 1.0005, 1.012, and 0.9831. These results indicate that, with our approach in processing OCTS and POLDER data, there are no obvious bias differences in the derived $[L_w(\lambda)]_N$ between the two sensors, whereas the noise differences are difficult to correct since they depend mainly on the sensor characteristics.

C. OCTS and POLDER Chlorophyll-a Comparisons

Figure 7 provides comparisons of chlorophyll-a concentration derived from OCTS and POLDER using the OC2 algorithm,[21] which was modified for OCTS and POLDER, over the Sargasso Sea and the Bermuda area. Fig. 7(a) shows results for the Sargasso sea, while Fig. 7(b) shows those of the Bermuda area. The color images are scaled logarithmically from 0.01 to 5 (mg m^{-3}), and the color scale is indicated at the bottom of Fig. 7(b). In Fig. 7, columns 1 and 2 are color images, respectively, for the OCTS and POLDER-derived chlorophyll-a concentrations, while column 3 shows a histogram comparison of the distributions between the two color images.

Over the Bermuda area (Fig. 7(b)), there were some in situ measurements which were acquired at about the same time as for some the OCTS and POLDER measurements. These data are archived in the SeaBASS data base. The in situ data were taken near the center of the Bermuda 3°×3° box area (center of the images). These in situ data are shown as vertical bars in the histograms in Fig. 7(b). Therefore, for the case of December 12, 1996, the OCTS and POLDER-derived chlorophyll values appear to be under-estimated, as compared with the in situ data. However, there were no retrievals from OCTS and POLDER over the center and top-most two-thirds part of the image box area. Therefore, the values from the satellites may not be representative for comparison with the in situ measurements. The same is also true for the case of June 10, 1997, where there were no retrievals for the bottom-most two-thirds part of the images. On the other hand, when coverage did coincide with field data as for both March 19, 1997 and May 7,

1997 both satellites compared well with in situ measurements. Note that in situ data for May 7, 1997 and June 10, 1997 were obtained one day earlier (May 6, 1997) and one day later (June 11, 1997), respectively.

There are obvious variations in the derived chlorophyll-a concentrations between OCTS and POLDER. However, it is found that, for the chlorophyll-a concentration comparison, the average ratio value (mode in histogram) of OCTS/POLDER for all the Sargasso Sea and the Bermuda area cases (total of 12) is 0.9907.

D. Discussion

In examining the results of the comparisons between OCTS and POLDER, it is clear that there are no bias differences in the derived products between the two sensors. However, it has been consistently shown that, compared to OCTS, the POLDER-derived ocean color data are often more noisy, in particular, for data derived from the POLDER 443-nm band. One possible reason for such variability could be due to POLDER sensor non-linearity.[35] Results have shown[35] that the POLDER sensor non-linear responses under-estimate radiance values at the lower radiance ranges, while they over-estimate values for the high radiance ranges. It was reported[35] that the POLDER 443 nm band has about a 3% non-linear variation from low to high radiances for ocean color measurements. Other bands also have non-linear responses, but with much smaller magnitudes.[35]

Some high sparkling values in the POLDER-derived ocean color products, however, are mostly from the cloud-edge effects, due to sub-pixel cloud contamination. With a low spatial resolution pixel, POLDER measurements are more likely to be contaminated by sub-pixel clouds. The cloud contaminated pixels could be mis-identified as clear because their radiance values are not high enough to trigger the cloud threshold.

6. Conclusion

We describe a procedure to vicariously calibrate OCTS and POLDER Level-1B data using the MOBY in situ measurements. It effectively bridges the OCTS and POLDER

Level-1B data through the use of a common set of MOBY in situ measurements. The vicarious calibration assumes the band 865 nm gain coefficients are not changed, while the visible bands are adjusted such that the derived normalized water-leaving radiances are forced to be equivalent to the MOBY in situ measurements. Using the derived gain coefficients, a consistent atmospheric correction algorithm is used to process OCTS and POLDER data from Level-1B to Level-2 products. Therefore, the differences in the OCTS and POLDER-derived ocean color products are mainly from the differences of the sensor characteristics, i.e., with this approach, the retrieved products would be identical if the two sensors were identical.

We demonstrate the efficacy of vicariously re-calibrating OCTS and POLDER with a common in situ data set and using a consistent atmospheric correction algorithm for data processing. Both the OCTS and POLDER-derived normalized water-leaving radiances compare reasonably well with independent in situ data. Over the Sargasso Sea and the Bermuda area, the ocean color products derived from OCTS have a good agreement with data from POLDER measurements. It is particularly important that there are no bias differences between the OCTS and POLDER-derived ocean color data, i.e., the overall ratio values between the OCTS and POLDER-derived normalized water-leaving radiances at 443, 490, and 565 nm are: 1.0005, 1.012, and 0.9831, while it is 0.9907 for the ratio value in the derived chlorophyll-a concentration. However, the noise differences, which are usually inherited from sensor characteristics, are difficult to remove. These noise differences can be possibly reduced using data averaging schemes (e.g. averaging Level-2 data to Level-3 products). It is found that the POLDER-derived $[L_w(\lambda)]_N$ are usually more noisy than those of OCTS, in particular, for the 443 nm band products. This most likely resulted from the POLDER sensor non-linearity response problem.[35] On the other hand, effects of the sub-pixel cloud contamination around cloud edge lead to high sparkling values in the POLDER-retrieved ocean color products.

The OCTS and POLDER data processing procedures and algorithms are planned to be implemented in MSL12 within the SeaDAS software,[12] which is freely available. Therefore, interested scientists can process OCTS and POLDER data using the widely distributed SeaDAS software package.

REFERENCES

1. J. Tanii, T. Machida, H. Ayada, Y. Katsuyama, J. Ishida, N. Iwasaki, Y. Tange, Y. Miyachi and R. Sato, "Ocean Color and Temperature Scanner (OCTS) for ADEOS," SPIE **1490**, 200-206 (1991).

2. P. Y. Deschamps, F. M. Bréon, M. Leroy, A. Podaire, A. Bricaud, J. C. Buriez and G. Sèze, "The POLDER Mission: Instrument Characteristics and Scientific Objectives," IEEE Trans. Geosc. Rem. Sens. **32**, 598-615 (1994).

3. C. R. McClain and G. S. Fargion, "SIMBIOS Project 1999 Annual Report," NASA Goddard Space Flight Center, Greenbelt, MD, SIMBIOS Technical Report Series NASA tech. memo. 1999-209486, 1999.

4. M. Wang and B. A. Franz, "Comparing the ocean color measurements between MOS and SeaWiFS: A vicarious intercalibration approach for MOS," IEEE Trans. Geosci. Remote Sens. **38**, 184-197 (2000).

5. G. Zimmermann and A. Neumann, "The Spaceborne Imaging Spectrometer MOS for Ocean Remote Sensing," Proceedings of the 1st International Workshop on MOS-IRS and Ocean Color, DLR, Institute of Space Sensor Technology, Berlin, April 28-30, pp. 1-9, 1997.

6. S. B. Hooker, W. E. Esaias, G. C. Feldman, W. W. Gregg and C. R. McClain, "An Overview of SeaWiFS and Ocean Color," S.B. Hooker and E.R. Firestone, Eds., NASA Goddard Space Flight Center, Greenbelt, Maryland, 24 pp., Vol. 1 of SeaWiFS Technical Report Series NASA tech. memo. 104566, 1992.

7. C. R. McClain, M. L. Cleave, G. C. Feldman, W. W. Gregg, S. B. Hooker and N. Kuring, "Science Quality SeaWiFS Data for Global Biosphere Research," *Sea Techno.*, pp. 10-16, September 1998.

8. D. K. Clark, H. R. Gordon, K. J. Voss, Y. Ge, W. Broenkow and C. Trees, "Validation of atmospheric correction over the ocean," J. Geophys. Res. **102**, 17,209-17,217 (1997).

9. H. R. Gordon and M. Wang, "Retrieval of water-leaving radiance and aerosol optical thickness over the oceans with SeaWiFS: A preliminary algorithm," Appl. Opt. **33**, 443-452 (1994).

10. H. Fukushima, A. Higurashi, Y. Mitomi, T. Nakajima, T. Noguchi, T. Tanaka and M. Toratani, "Correction of atmospheric effects on ADEOS/OCTS ocean color data: Algorithm description and evaluation of its performance," J. Oceanogr. **54**, 417-430 (1998).

11. H. R. Gordon, "Atmospheric correction of ocean color imagery in the Earth Observing System era," J. Geophys. Res. **102**, 17,081-17,106 (1997).

12. K. Baith, R. Lindsay, G. Fu and C. R. McClain, "SeaDAS: A data analysis system for ocean color satellite sensors," in *Eos, Trans. Am. Geophys. U.*, in press.

13. W. W. Gregg, "Initial analysis of ocean color data from the ocean color and temperature scanner. I. Imagery analysis," Appl. Opt. **38**, 476-485 (1999).

14. M. Shimada, H. Oaku, Y. Mitomi, H. Murakami, Y. Nakamura, J. Ishizaka, H. Kawamura, T. Tanaka, M. Kishino and H. Fukushima, "Calibration and validation of the ocean color version-3 product from ADEOS OCTS," J. Oceanogr. **54**, 401-416 (1998).

15. F. S. Patt and W. W. Gregg, "Exact closed-form geolocation algorithm for earth survey sensors," Int. J. Remote Sens. **15**, 3719-3734 (1994).

16. F. S. Patt, R. H. Woodward and W. W. Gregg, "An automated method for navigation assessment for earth survey sensors using island targets," Int. J. Remote Sens. **18**, 3311-3336 (1997).

17. H. R. Gordon and M. Wang, "Influence of oceanic whitecaps on atmospheric correction of ocean-color sensor," Appl. Opt. **33**, 7754-7763 (1994).

18. D. Antoine and A. Morel, "A multiple scattering algorithm for atmospheric correction of remotely sensed ocean colour (MERIS instrument): principle and implementation for atmospheres carrying various aerosols including absorbing ones," Int. J. Remote Sens. **20**, 1875-1916 (1999).

19. H. R. Gordon, O. B. Brown, R. H. Evans, J. W. Brown, R. C. Smith, K. S. Baker and D. K. Clark, "A semianalytic radiance model of ocean color," J. Geophys. Res. **93**, 10909-10924 (1988).

20. A. Morel, "Optical modeling of the upper ocean in relation to its biogenous matter content (case 1 waters)," J. of Geophys. Res. **93**, 10749-10768 (1988).

21. J. E. O'Reilly, S. Maritorena, B. G. Mitchell, D. A. Siegel, K. L. Carder, S. A. Garver, M. Kahru and C. R. McClain, "Ocean color chlorophyll algorithms for SeaWiFS," J. Geophys. Res. **103**, 24,937-24,953 (1998).

22. M. Wang, "A sensitivity study of SeaWiFS atmospheric correction algorithm: Effects of spectral band variations," Remote Sens. Environ. **67**, 348-359 (1999).

23. K. Ding and H. R. Gordon, "Analysis of the influence of O_2 A-band absorption on atmospheric correction of ocean color imagery," Appl. Opt. **34**, 2068-2080 (1995).

24. M. Wang, "Validation study of the SeaWiFS oxygen A-band absorption correction: comparing the retrieved cloud optical thicknesses from SeaWiFS measurements," Appl. Opt. **38**, 937-944 (1999).

25. M. Wang, "The SeaWiFS atmospheric correction algorithm updates," S.B. Hooker and E.R. Firestone, Eds., NASA Goddard Space Flight Center, Greenbelt, Maryland, p57-63, SeaWiFS Postlaunch Technical Report Series Vol. 9, NASA Tech. Memo. 2000-206892, 2000.

26. D. A. Siegel, M. Wang, S. Maritorena and W. Robinson, "Atmospheric correction of satellite ocean color imagery: the black pixel assumption," Appl. Opt. **39**, 3582-3591 (2000).

27. H. R. Gordon and M. Wang, "Surface roughness considerations for atmospheric correction of ocean color sensors. 1: The Rayleigh scattering component," Appl. Opt. **31**, 4247-4260 (1992).

28. M. Wang, "Effects of the sea surface wind speed on the SeaWiFS derived ocean color optical property data," Proceedings of Ocean Optics XV, Musée Océanographique, Monaco, October 16-20, 2000, , 2000.

29. M. Wang and S. Bailey, "Correction of the sun glint contamination on the SeaWiFS aerosol optical thickness retrievals," S.B. Hooker and E.R. Firestone, Eds., NASA Goddard Space Flight Center, Greenbelt, Maryland, p64-68, The SeaWiFS Post-launch Technical Report Series Vol. 9, NASA Tech. Memo. 2000-206892, 2000.

30. R. Frouin, M. Schwindling and P. Y. Deschamps, "Spectral reflectance of sea foam in the visible and near infrared: In situ measurements and remote sensing implications," J. Geophys. Res. **101**, 14,361-14,371 (1996).

31. K. D. Moore, K. J. Voss and H. R. Gordon, "Spectral reflectance of whitecaps: Instrumentation, calibration, and performance in coastal waters," J. Atmos. Ocean. Tech. **15**, 496-509 (1998).

32. K. D. Moore, K. J. Voss and H. R. Gordon, "Spectral reflectance of whitecaps: Their contribution to water-leaving radiance," J. of Geophys. Res. **105**, 6493-6499 (2000).

33. E. P. Shettle and R. W. Fenn, "Models for the Aerosols of the Lower Atmosphere and the Effects of Humidity Variations on Their Optical Properties," U.S. Air Force Geophysics Laboratory, Hanscom Air Force Base, Mass. AFGL-TR-79-0214, 1979.

34. M. Wang, B. A. Franz, R. A. Barnes and C. R. McClain, "Effects of spectral bandpass on SeaWiFS-retrieved near-surface optical properties of the ocean," Appl. Opt. **40**, 342-348 (2001).

35. B. Fougnie, O. Hagolle and F. Cabot, "In-flight measurement and correction of non-linearity of the POLDER-1's sensitivity," Proceedings of Physical Measurements & Signatures in Remote Sensing, Aussois, France, , pp. 211-219, 2001.

36. H. R. Gordon, "In-orbit calibration strategy for ocean color sensors," Rem. Sens. Environ. **63**, 265-278 (1998).

37. W. Robinson and M. Wang, "Vicarious calibration of the SeaWiFS band 7," S.B. Hooker and E.R. Firestone, Eds., NASA Goddard Space Flight Center, Greenbelt, Maryland, p38-42, SeaWiFS Postlaunch Technical Report Series Vol. 9, NASA Tech. Memo. 2000-206892, 2000.

38. J. R. E. Eplee and C. R. McClain, "MOBY Data Analysis for the Vicarious Calibration of SeaWiFS Bands 1-6," S.B. Hooker and E.R. Firestone, Eds., NASA Goddard Space Flight Center, Greenbelt, Maryland, p43-50, SeaWiFS Postlaunch Technical Report Series Vol. 9, NASA Tech. Memo. 2000-206892, 2000.

39. O. Hagolle, P. Goloub, P. Y. Deschamps, H. Cosnefroy, X. Briottet, T. Bailleul, J. M. Nicolas, F. Parol, B. Lafrance and M. Herman, "Results of POLDER in-flight calibration," IEEE Trans. Geosci. Remote Sens. **37**, 1550-1566 (1999).

Figure Captions

Figure 1. The OCTS and POLDER 765 nm band spectral response functions compared with that of SeaWiFS.

Figure 2. Spectral bandpass correction factor $r(\lambda)$ as a function of the sensor-derived two-band ratio values in the normalized water-leaving radiances between wavelengths 490 and 565 nm for (a) the OCTS bands 412, 443, 490, 520, and 565 nm and (b) the POLDER bands 443, 490, and 565 nm. The curves are the lest-squares fit.

Figure 3. The OCTS-derived ocean color parameters compared with the in situ measurements for (a) $[L_w(\lambda)]_N$ with OCTS NASDA Level-1B data; (b) $[L_w(\lambda)]_N$ with OCTS Wallops Level-0 data; (c) ratio $[L_w(\lambda)]_N / [L_w(565)]_N$ with OCTS NASDA Level-1B data; and (d) ratio $[L_w(\lambda)]_N / [L_w(565)]_N$ with OCTS Wallops Level-0 data. Each plot indicates a linear fit coefficients of slope, intercept (Int), and the correlation coefficient (R).

Figure 4. The POLDER-derived ocean color parameters compared with the in situ measurements from POLDER CNES Level-1B data for (a) $[L_w(\lambda)]_N$ and (b) ratio $[L_w(\lambda)]_N / [L_w(565)]_N$ values. Each plot indicates a linear fit coefficients of slope, intercept (Int), and the correlation coefficient (R).

Figure 5. The OCTS-retrieved normalized water-leaving radiance images at wavelengths 443, 490, and 565 nm compared with those derived from POLDER measurements for ocean water over (a) the Sargasso Sea from Nov. 20, 1996 to May 20, 1997 and (b) the Bermuda area from Dec. 12, 1996 to June 10, 1997.

Figure 6. The histogram (%) of the OCTS-retrieved normalized water-leaving radiances at wavelengths 443, 490, and 565 nm compared with those from POLDER measurements as in Fig. 5 for (a)-(g) the Sargasso Sea from Nov. 20, 1996 to May 20, 1997 and (h)-(i) the Bermuda area from Dec. 12, 1996 to June 10, 1997.

Figure 7. The OCTS-retrieved chlorophyll-a concentration compared with those derived from POLDER measurements for (a) the Sargasso Sea from Nov. 20, 1996 to April 14, 1997 and (b) the Bermuda area from Dec. 12, 1996 to June 10, 1997. Some of the in situ measurements are also indicated as vertical bars in the histograms over the Bermuda area in (b).

TABLE 1. The derived vicarious gain coefficients for OCTS and POLDER spectral bands.

Wavelength (nm)	Gain Coefficient $G^{(VC)}(\lambda)$	
	OCTS	POLDER
412	1.12426	—
443	1.01539	1.06465
490	0.95084	1.02350
520	1.01784	—
565	1.03255	0.97541
670	1.00859	1.01845
765	0.92093	1.02946
865	1.00000	1.00000

TABLE 2(a). The OCTS/POLDER comparisons in the retrieved $[L_w(\lambda)]_N$ (mode value) over the Sargasso Sea from Nov. 20, 1996 to May 20, 1997.

Date	$[L_w(443)]_N$[†]			$[L_w(490)]_N$[†]			$[L_w(565)]_N$[†]		
	OCTS	POLDER	%Diff	OCTS	POLDER	%Diff	OCTS	POLDER	%Diff
Nov. 20, 1996	1.8015	1.7500	2.90	1.2209	1.1503	5.95	0.1975	0.2844	-36.07
Dec. 19, 1996	1.5489	1.4115	9.28	1.0491	1.1101	-5.65	0.1519	0.1606	-5.54
Jan. 26, 1997	1.6381	1.7798	-8.29	1.1048	1.0874	1.60	0.1643	0.1587	3.46
Feb. 17, 1997	1.8567	1.7216	7.55	1.1591	1.1659	-0.58	0.1841	0.2048	-10.62
Mar. 11, 1997	1.8705	2.2018	-16.27	1.1722	1.2684	-7.89	0.1717	0.2077	-18.98
Apr. 14, 1997	2.0278	2.0893	-2.99	1.2324	1.2880	-4.41	0.1872	0.1877	-0.22
May 20, 1997	1.9583	2.0156	-2.88	1.1064	1.1901	-7.29	0.1576	0.1525	3.29

[†]unit of $(mW\ cm^{-2}\ \mu m^{-1}\ sr^{-1})$.

TABLE 2(b). The OCTS/POLDER comparisons in the retrieved $[L_w(\lambda)]_N$ (mode value) over the Bermuda area from Dec. 12, 1996 to June 10, 1997.

Date	$[L_w(443)]_N$[†]			$[L_w(490)]_N$[†]			$[L_w(565)]_N$[†]		
	OCTS	POLDER	%Diff	OCTS	POLDER	%Diff	OCTS	POLDER	%Diff
Dec. 12, 1996	1.4346	0.9627	39.37	1.0865	0.9672	11.62	0.2093	0.1777	16.33
Mar. 19, 1997	1.4925	1.5656	-4.78	1.0410	1.0329	0.78	0.2104	0.2530	-18.33
May 3, 1997	1.6149	1.9393	-18.25	1.1171	1.1603	-3.79	0.1616	0.1515	6.45
May 7, 1997	1.7566	1.8485	-5.10	1.1937	1.0473	13.07	0.2121	0.1515	33.33
June 10, 1997	1.3194	1.5309	-14.84	1.1024	1.0383	5.99	0.1616	0.1818	-11.76

[†]unit of $(mW\ cm^{-2}\ \mu m^{-1}\ sr^{-1})$.
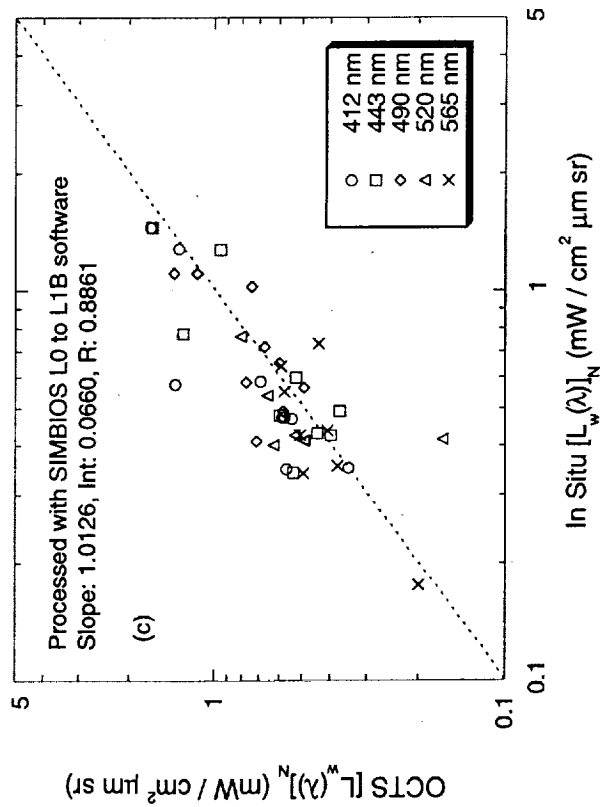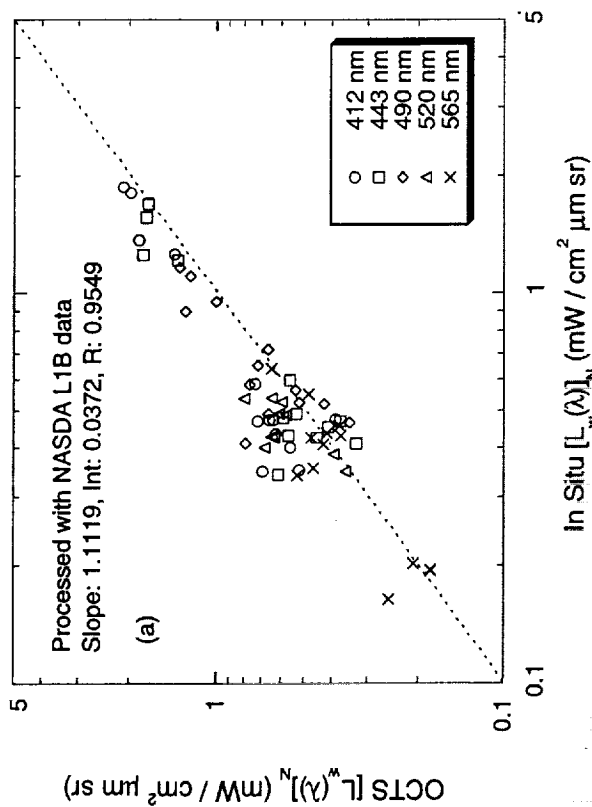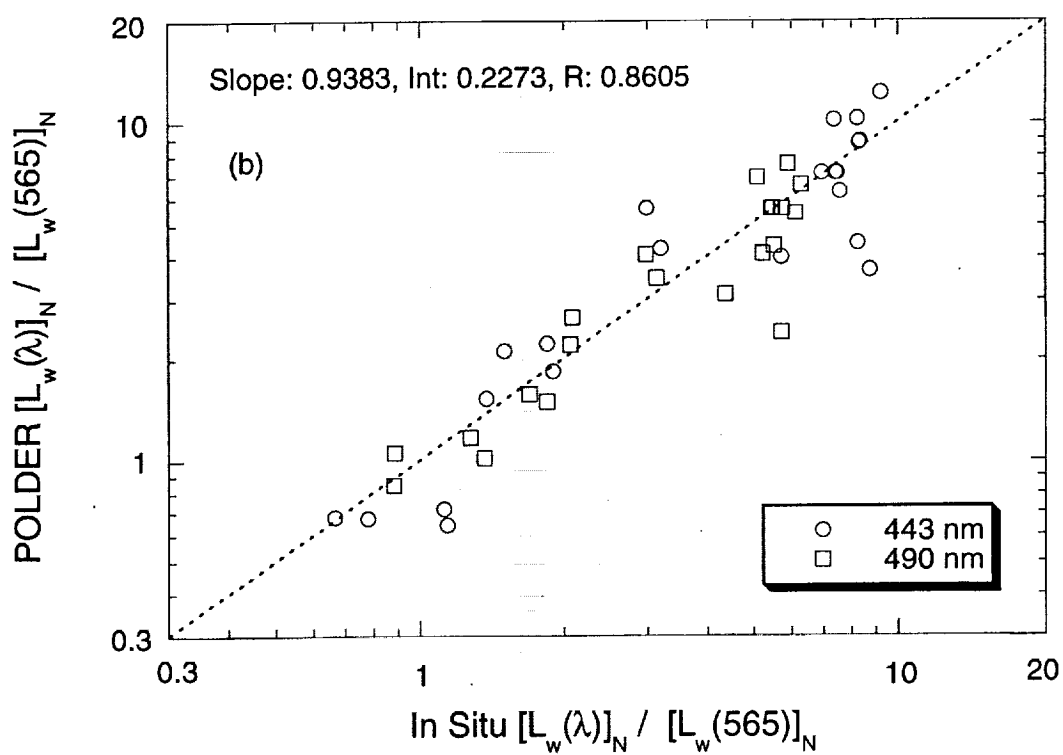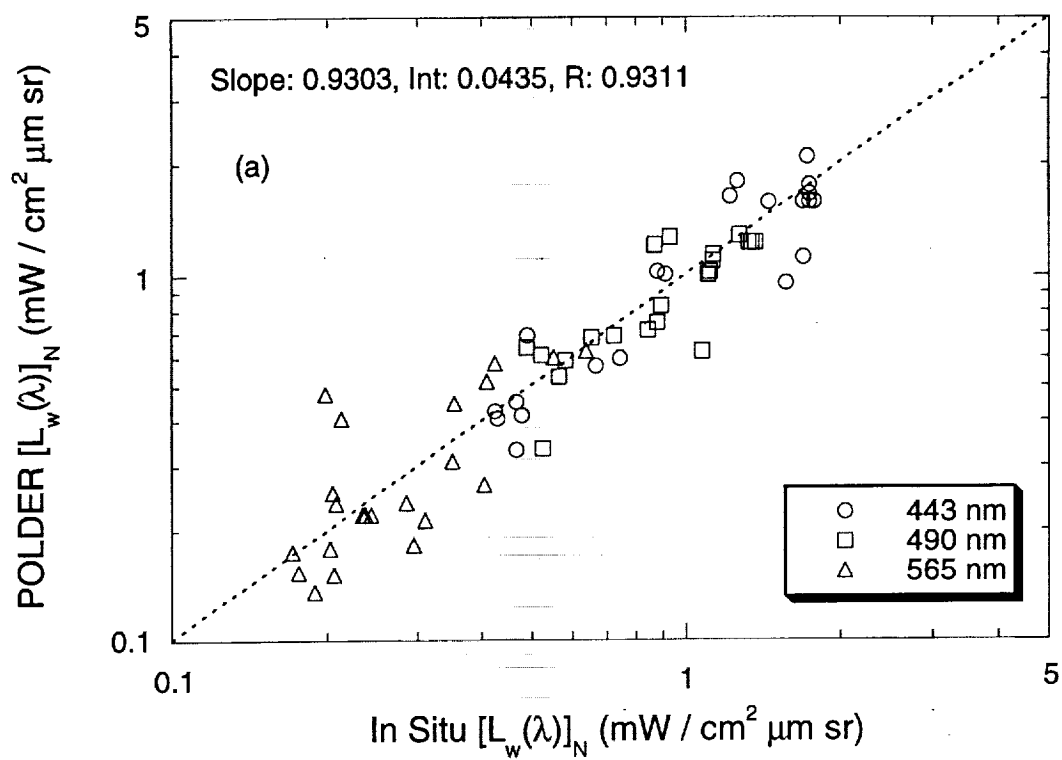
Spectral 765 nm Band
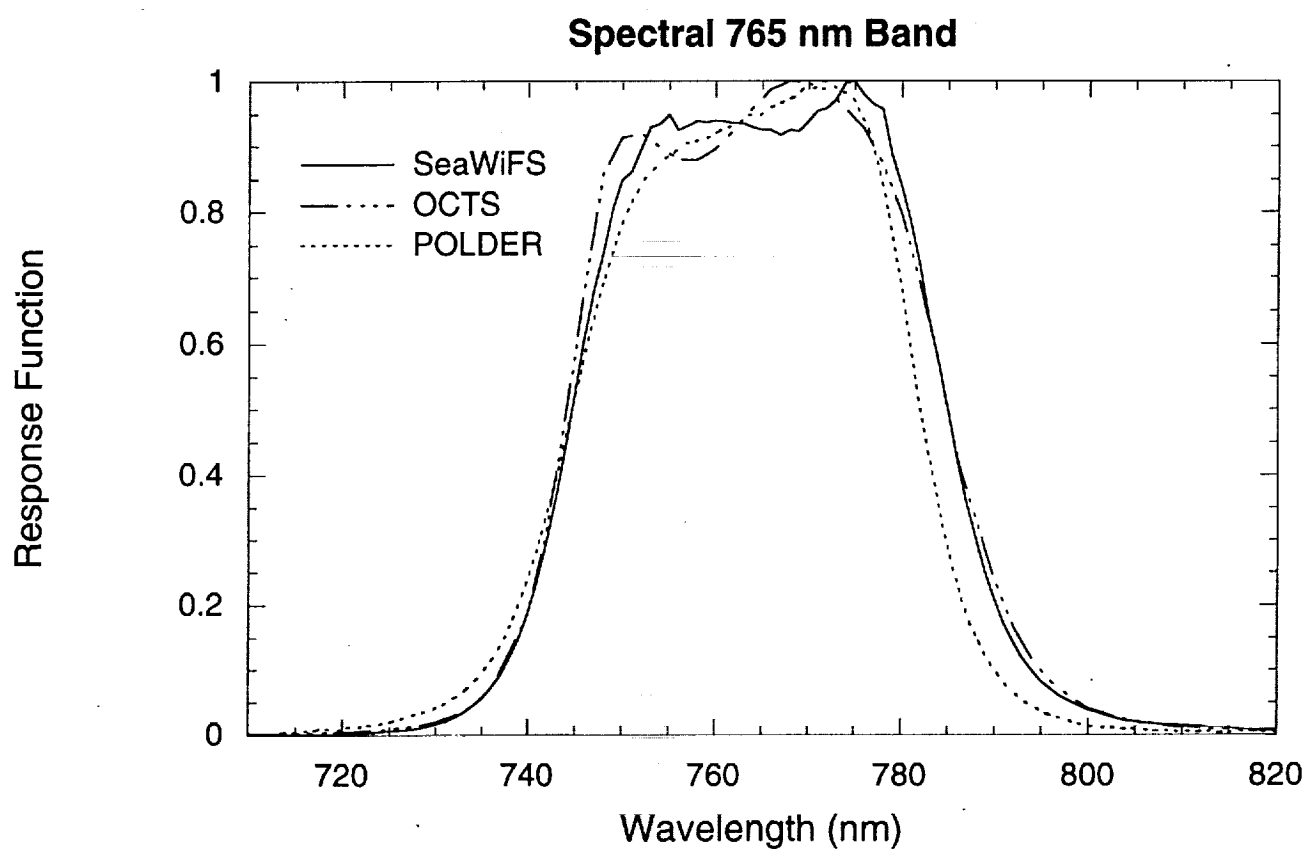
Fig. 1
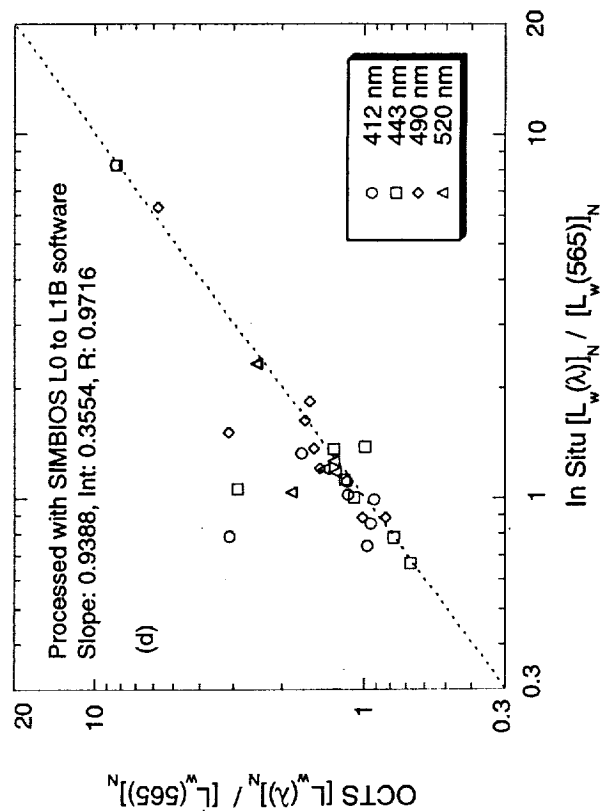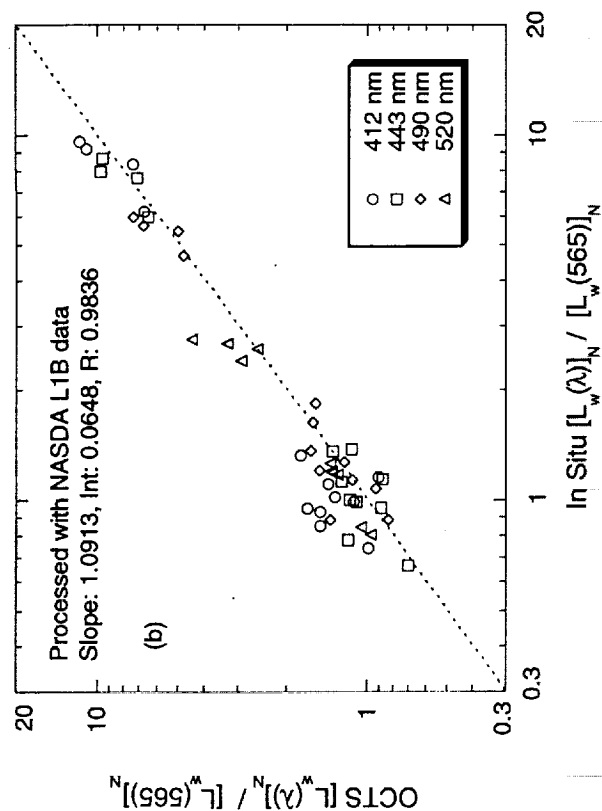
Fig. 3

Fig. 4

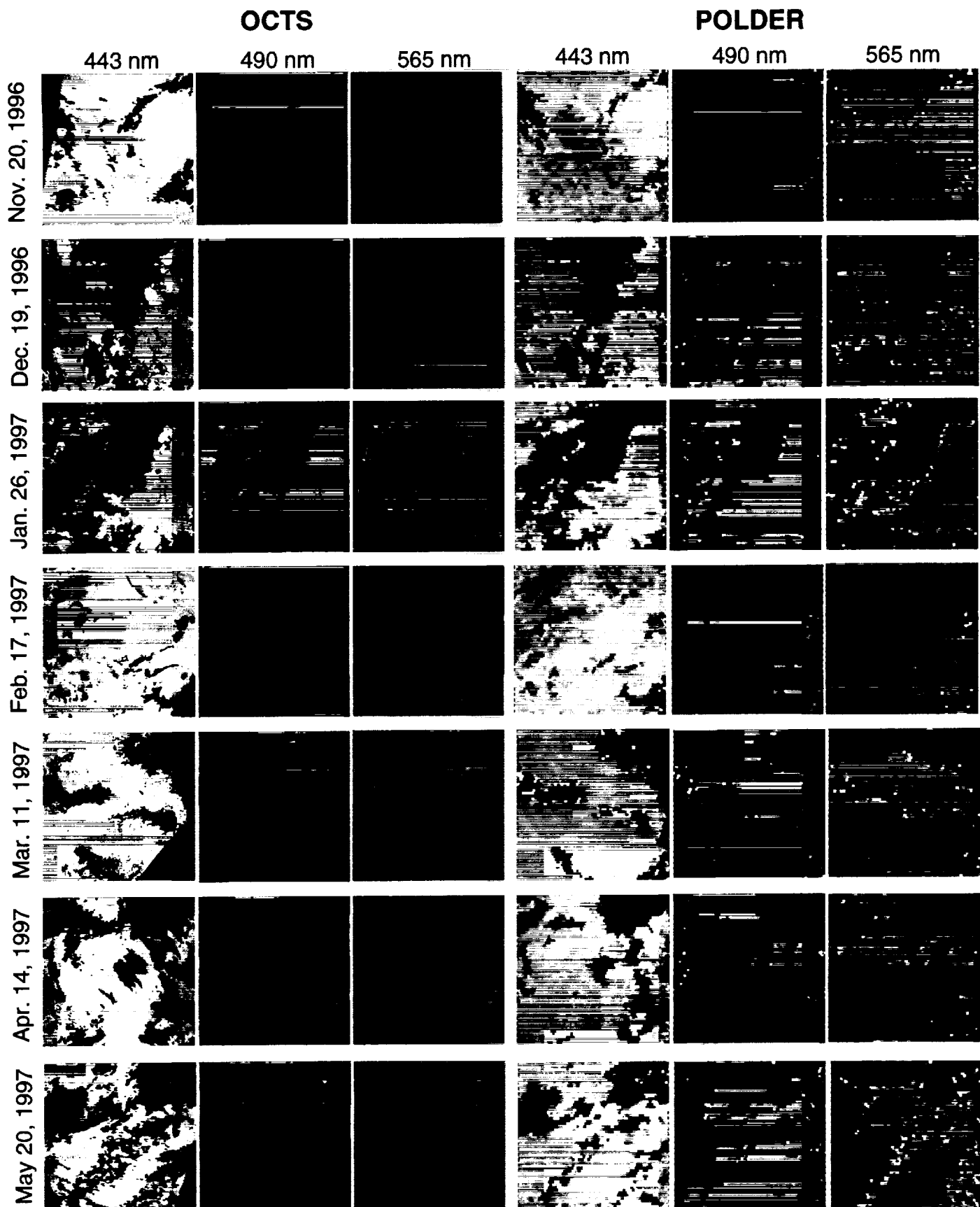# OCTS/POLDER $[L_w(\lambda)]_N$ Comparisons (Sargasso Sea)

Fig. 5(a)

OCTS/POLDER $[L_w(\lambda)]_N$ Comparisons (Bermuda)

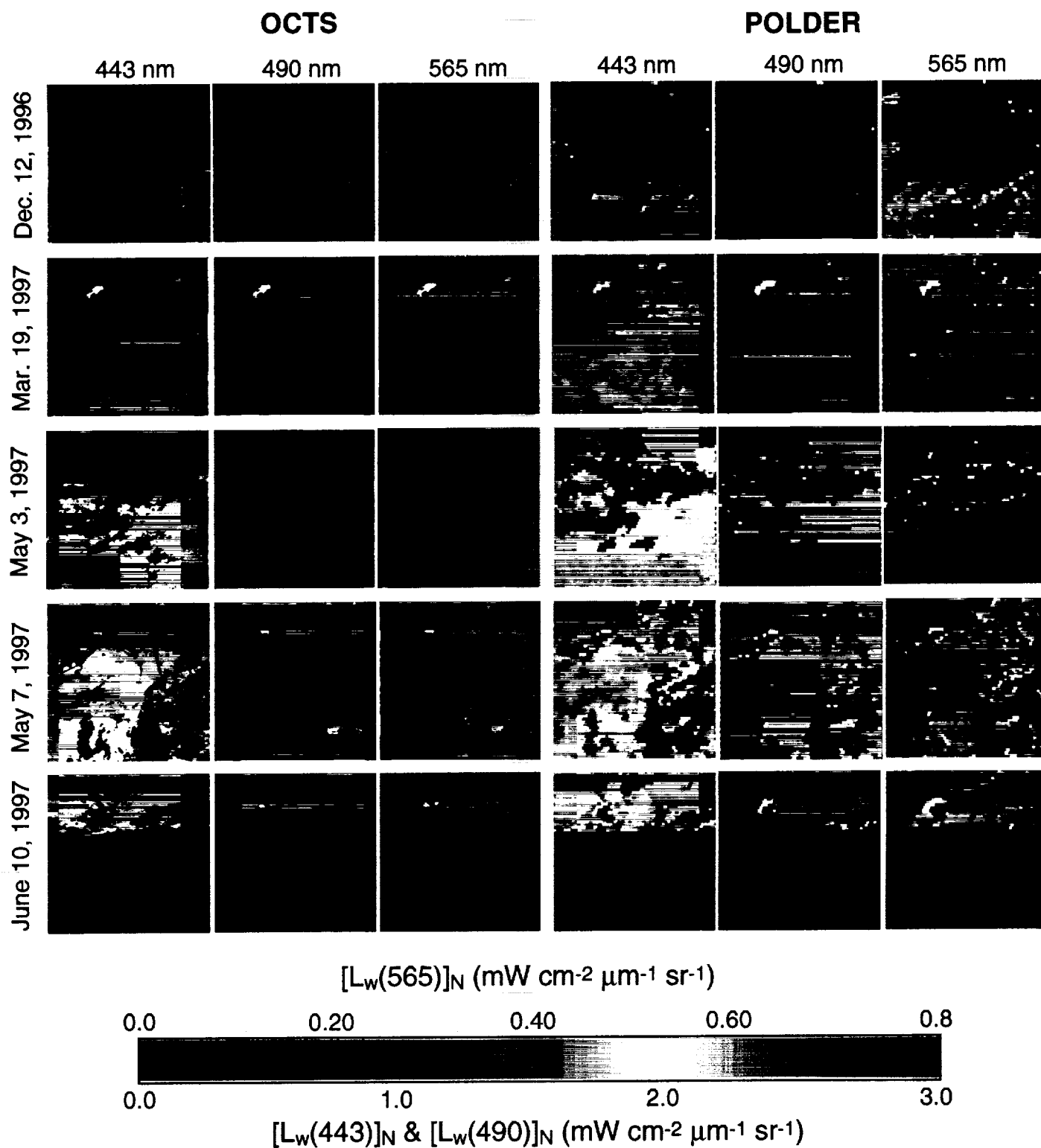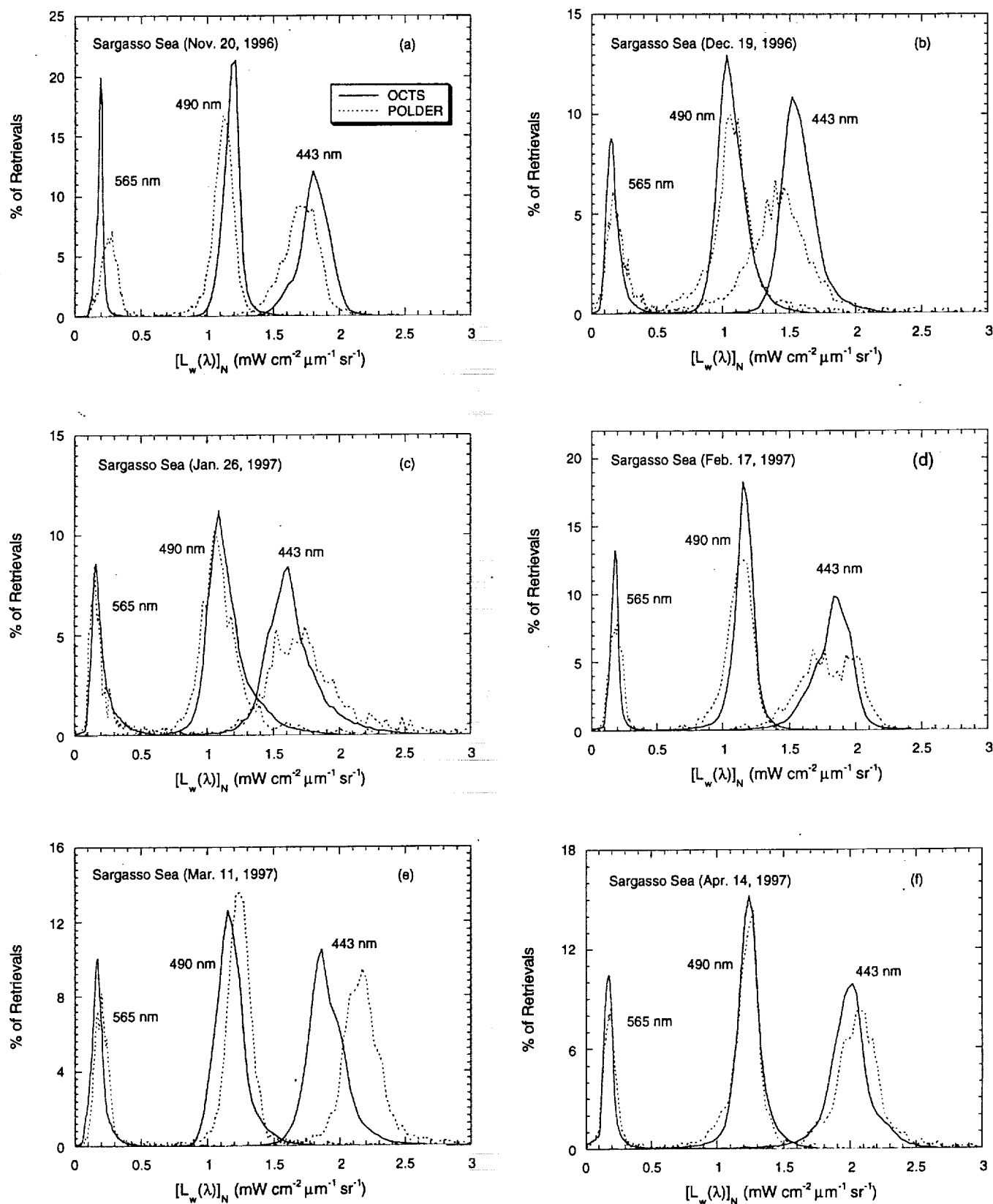|	OCTS			POLDER		
	443 nm	490 nm	565 nm	443 nm	490 nm	565 nm

$[L_w(565)]_N$ (mW cm⁻² μm⁻¹ sr⁻¹)

0.0	0.20	0.40	0.60	0.8

0.0	1.0	2.0	3.0

$[L_w(443)]_N$ & $[L_w(490)]_N$ (mW cm⁻² μm⁻¹ sr⁻¹)

Fig. 5 (b)

Fig. 6 (a) - (f)
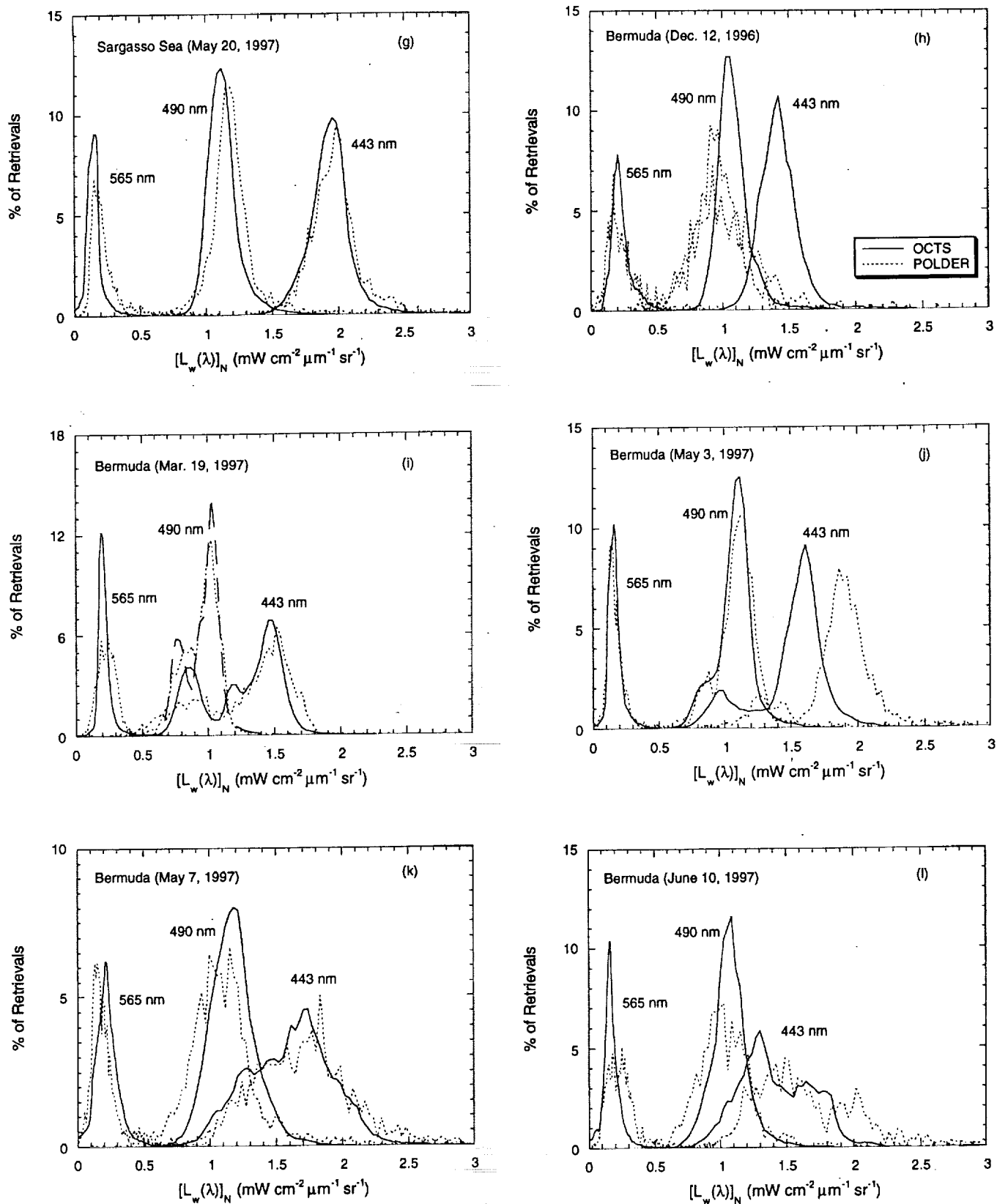
Fig. 6 (g) - (l)

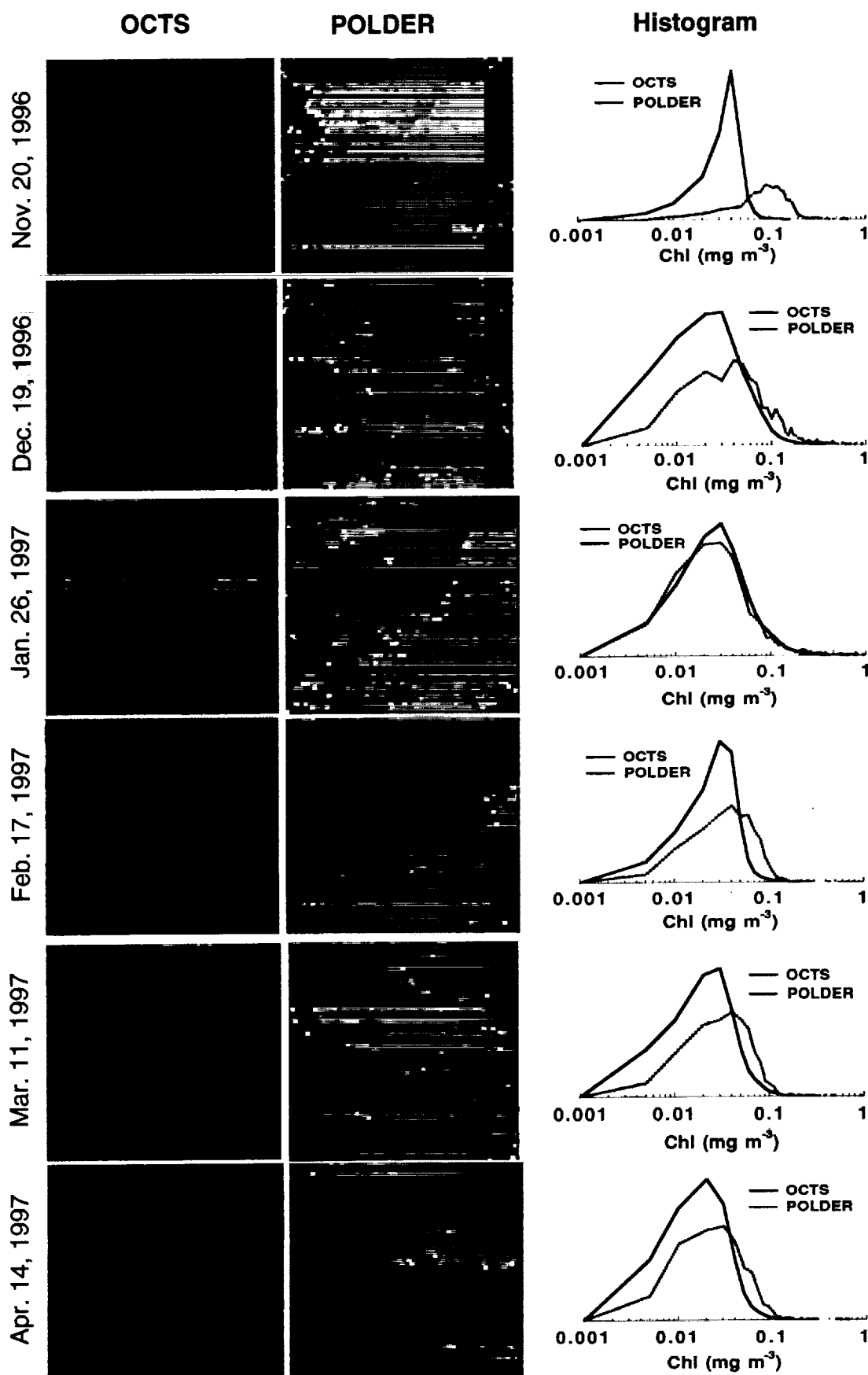OCTS/POLDER Chlorophyll-a Comparisons (Sargasso Sea)

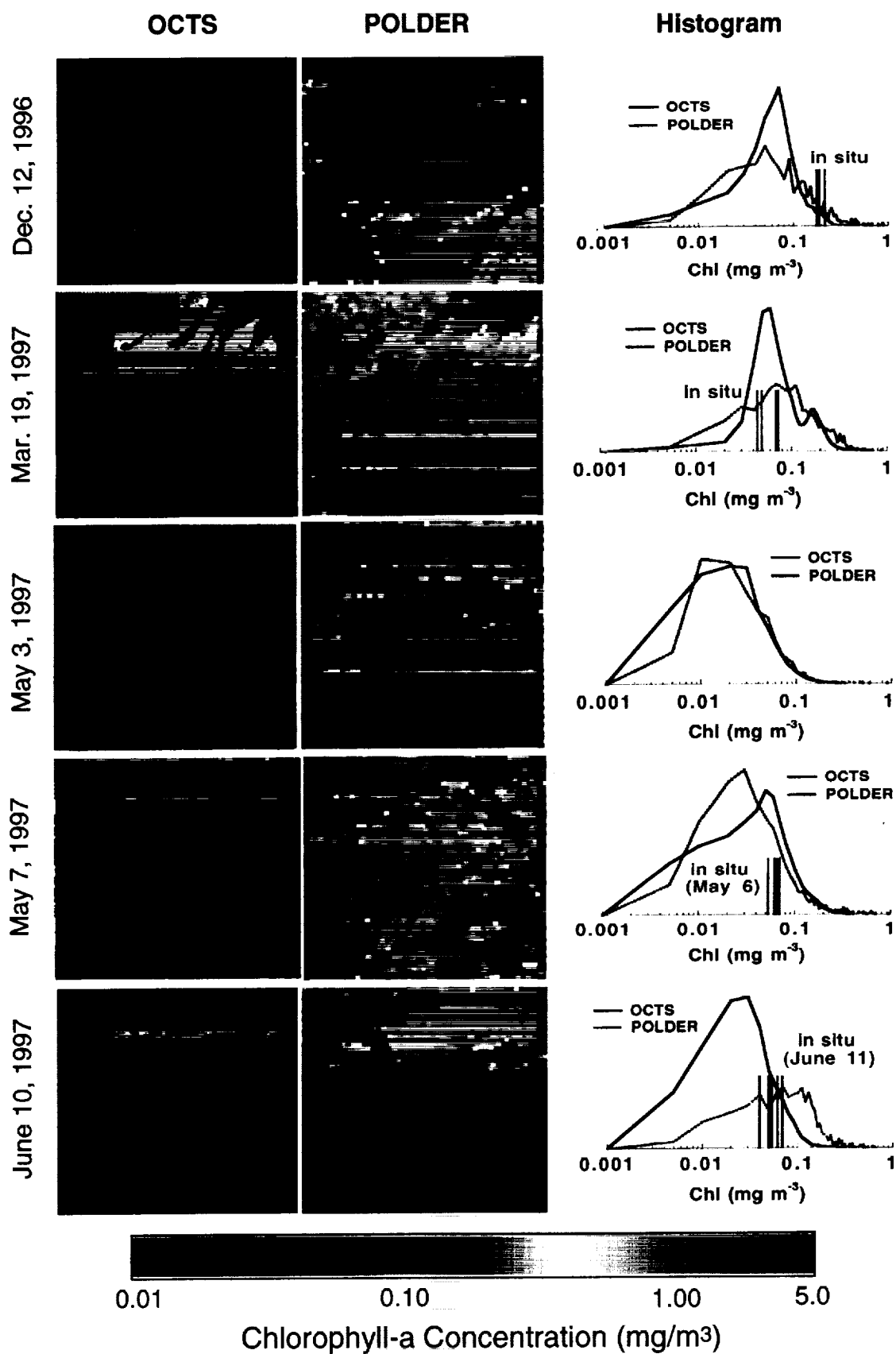Fig. 7 (a)

OCTS/POLDER Chlorophyll-a Comparisons (Bermuda)

Fig. 7(b)

Ocean Color Optical Property Data Derived from OCTS and POLDER: A Comparison Study

Menghua Wang[1], Alice Isaacman[2], Bryan A. Franz[2], and
Charles R. McClain

Code 970.2, NASA Goddard Space Flight Center
Greenbelt, Maryland 20771, USA
[1]University of Maryland Baltimore County
[2]SAIC General Sciences Corporation

SIGNIFICANT RESULTS

We describe our efforts in studying and comparing the ocean color data derived from the Japanese Ocean Color and Temperature Scanner (OCTS) and the French Polarization and Directionality of the Earth's Reflectances (POLDER). We describe our approach in developing consistent data processing algorithms for both OCTS and POLDER and using a common in situ data set to vicariously calibrate the two sensors. Therefore, the OCTS and POLDER-measured radiances are effectively bridged through common in situ measurements. The ocean color data from OCTS and POLDER can therefore be compared and merged in the sense that there is no significant bias between two.

This work falls under the Long-Term Climate Variability Science Priority.